NUMERICAL AND THEORETICAL STUDIES OF ROUGH SURFACE SCATTERING

Final Report

Eric I. Thorsos

December 28, 1994

U.S. ARMY RESEARCH OFFICE

Grant Number: DAAL03-92-G-0102

Applied Physics Laboratory
College of Ocean and Fishery Sciences
University of Washington

Approved for Public Release;
Distribution Unlimited

DISCLAIMER NOTICE

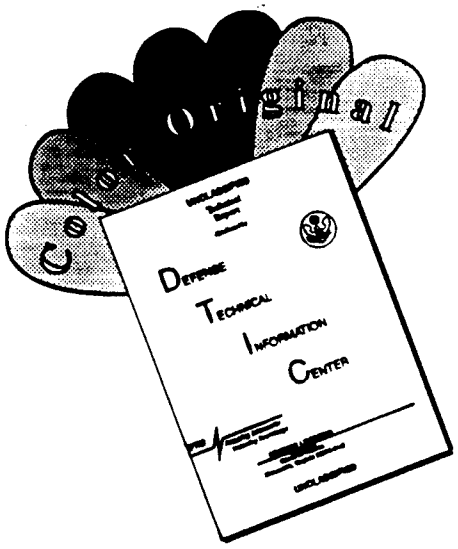

THIS DOCUMENT IS BEST QUALITY AVAILABLE. THE COPY FURNISHED TO DTIC CONTAINED A SIGNIFICANT NUMBER OF COLOR PAGES WHICH DO NOT REPRODUCE LEGIBLY ON BLACK AND WHITE MICROFICHE.

MASTER COPY KEEP THIS COPY FOR REPRODUCTION PURPOSES

REPORT DOCUMENTATION PAGE

Form Approved
OMB No. 0704-0188

1. AGENCY USE ONLY (Leave blank)	2. REPORT DATE	3. REPORT TYPE AND DATES COVERED
	December 1994	Final 1 Apr 92 - 30 Sep 94

4. TITLE AND SUBTITLE

Numerical and Theoretical Studies of Rough Surface Scattering

5. FUNDING NUMBERS

DAAL03-92-G-0102

6. AUTHOR(S)

Eric I. Thorsos

7. PERFORMING ORGANIZATION NAME(S) AND ADDRESS(ES)

University of Washington
Seattle, WA 98105-6698

8. PERFORMING ORGANIZATION REPORT NUMBER

9. SPONSORING / MONITORING AGENCY NAME(S) AND ADDRESS(ES)

U. S. Army Research Office
P. O. Box 12211
Research Triangle Park, NC 27709-2211

10. SPONSORING / MONITORING AGENCY REPORT NUMBER

ARO 29404.1-GS

11. SUPPLEMENTARY NOTES

The view, opinions and/or findings contained in this report are those of the author(s) and should not be construed as an official Department of the Army position, policy, or decision, unless so designated by other documentation.

12a. DISTRIBUTION / AVAILABILITY STATEMENT

Approved for public release; distribution unlimited.

12b. DISTRIBUTION CODE

13. ABSTRACT *(Maximum 200 words)*

The goal of this project was to improve our understanding of electromagnetic scattering from conducting rough surfaces when the roughness is small in comparison with the radiation wavelength. Research was conducted in two related areas for p-polarized scattering from conducting surfaces: (1) the generation of surface waves, and (2) the development of renormalized perturbation theory for scattering from perfectly conducting surfaces. To understand the excitation of surface waves better, a numerical method was developed for displaying the field near the surface; surface waves can then be shown explicitly. The method is based on integral equation solutions, and no fundamental approximations are required. The existence of surface waves for p-polarized scattering leads to difficulties in theoretical treatments of scattering from conductors. This work is specialized to the case of scattering from perfect conductors, for which the theoretical problems are most evident. A renormalized perturbation theory is implemented that is free from the deficiencies inherent in standard perturbation theory. The renormalized perturbation theory is extended beyond lowest order, and comparisons with exact integral equation results show that this approach yields predictions for the bistatic scattering cross section that are accurate over a broad range of surface parameters.

14. SUBJECT TERMS

Electromagnetic scattering from rough surfaces, electromagnetic surface waves, renormalized perturbation theiry

15. NUMBER OF PAGES

31

16. PRICE CODE

17. SECURITY CLASSIFICATION OF REPORT	18. SECURITY CLASSIFICATION OF THIS PAGE	19. SECURITY CLASSIFICATION OF ABSTRACT	20. LIMITATION OF ABSTRACT
UNCLASSIFIED	UNCLASSIFIED	UNCLASSIFIED	UL

NUMERICAL AND THEORETICAL STUDIES OF ROUGH SURFACE SCATTERING

Final Report

Eric I. Thorsos

December 28, 1994

U.S. ARMY RESEARCH OFFICE

Grant Number: DAAL03-92-G-0102

Applied Physics Laboratory
College of Ocean and Fishery Sciences
University of Washington

ABSTRACT

The goal of this project was to improve our understanding of electromagnetic scattering from conducting rough surfaces when the roughness is small in comparison with the radiation wavelength. Research was conducted in two related areas for p-polarized scattering from conducting surfaces: (1) the generation of surface waves, and (2) the development of renormalized perturbation theory for scattering from perfectly conducting surfaces. To understand the excitation of surface waves better, a numerical method was developed for displaying the field near the surface; surface waves can then be shown explicitly. The method is based on integral equation solutions, and no fundamental approximations are required. The existence of surface waves for p-polarized scattering leads to difficulties in theoretical treatments of scattering from conductors. This work is specialized to the case of scattering from perfect conductors, for which the theoretical problems are most evident. A renormalized perturbation theory is implemented that is free from the deficiencies inherent in standard perturbation theory. The renormalized perturbation theory is extended beyond lowest order, and comparisons with exact integral equation results show that this approach yields predictions for the bistatic scattering cross section that are accurate over a broad range of surface parameters.

Contents

List of Figures

1. Problem Statement

The goal of this project was to improve our understanding of electromagnetic scattering from conducting rough surfaces, when the roughness is small in comparison with the radiation wavelength. Research has been conducted on two related areas for p-polarized scattering from conducting surfaces: (1) the generation of surface waves, and (2) the development of renormalized perturbation theory for scattering from perfectly conducting surfaces. For both topics, use has been made of the exact integral equation method restricted to one-dimensional (1-D) surfaces, and the restriction to 1-D surfaces has been made throughout in the analytic development as well.

Surface waves can be generated when p-polarized light (electric vector in the plane of incidence) scatters from good or perfect conductors with small roughness. To understand the excitation of surface waves better, a numerical method has been developed for displaying the field near the surface; surface waves can then be shown explicitly. The method is based on integral equation solutions, and no fundamental approximations are required. An outline of the numerical method and a discussion of results will be given.

The existence of surface waves for p-polarized scattering leads to difficulties in theoretical treatments of scattering from conductors. Here we specialize to the case of scattering from perfect conductors, for which the theoretical problems are most evident. When standard perturbation theory is applied to this case (the Neumann boundary condition problem), lowest-order results have unphysical properties near grazing (i.e., at angles of incidence or scattering near $\pm 90°$) and therefore must be incorrect near grazing. When standard perturbation theory is taken to second order, the expression for the scattering cross section diverges.[1] Building on theoretical work of A.A. Maradudin and colleagues,[2-5] a renormalized perturbation theory has been developed and implemented that is free from the deficiencies just mentioned. The goal has been to develop a perturbation theory with an implementation capable of giving accurate results for kh up to 0.5, where k is the radiation wavenumber and where h is the rms height of the surface roughness. Perturbation theory, if taken beyond lowest order, is valid for s-polarized scattering from perfect conductors (Dirichlet boundary condition) up to about this level of roughness.[6] Comparisons with exact integral equation results show that this goal has now been essentially reached for the Neumann boundary condition. An outline will be given of the renormalized perturbation theory followed by a discussion of implementation issues and a comparison with integral equation results.

2. Field Visualization in P-Polarized Scattering

We consider scattering from both perfect and good conductors. For perfect conductors, surface roughness is required for surface waves to exist. For good conductors, surface roughness can couple energy from volume propagating waves into surface waves, but after the surface wave has been generated, roughness is not necessary for the surface wave to exist. By displaying the near-surface fields, we can study the properties of surface waves for both good and perfect conductors.

2.1 Numerical method

The integral equations given below are equivalent to those derived by Maradudin et al.[7] We are concerned with the scattering of p-polarized light from a rough metal surface. Time harmonic

fields are assumed, and the time dependence is omitted. The plane of incidence is the x-z plane, and the rough surface profile is defined by $z = f(x)$, where the mean surface height is zero and where the z axis is directed upward from the metal into a vacuum. For p-polarized scattering from a 1-D surface, the y component is the only nonvanishing component of the magnetic field, which is denoted by $H(\mathbf{r})$ where $\mathbf{r}$ is a 2-D position vector. We wish to solve for $H(\mathbf{r})$ in the vicinity of the surface when a field $H_{\text{inc}}(\mathbf{r})$ is incident on the metal from the vacuum side of the interface.

If the metal is a perfect conductor, the field vanishes inside the conductor, and the boundary condition on the rough surface is

$$\frac{\partial H(\mathbf{r})}{\partial n} = 0 , \tag{1}$$

where $\partial/\partial n = \hat{\mathbf{n}} \cdot \nabla$, with $\hat{\mathbf{n}}$ a unit vector normal to the surface and directed from the metal to the vacuum. The solution of the following integral equation gives $H(\mathbf{r})$ on $z = f(x)$

$$H(\mathbf{r}) = 2H_{\text{inc}}(\mathbf{r}) + 2\int_s \frac{\partial G_0(\mathbf{r}, \mathbf{r}')}{\partial n'} H(\mathbf{r}')\, ds' \cdot \tag{2}$$

In (2) both $\mathbf{r}$ and $\mathbf{r}'$ are confined to the rough surface, and $ds' = \gamma(x')dx'$, where $\gamma^2(x) = 1 + (df(x)/dx)^2$. Also in (2) G_0 is the free space Green's function in the vacuum

$$G_0(\mathbf{r}, \mathbf{r}') = \frac{i}{4} H_0^{(1)}(k|\mathbf{r} - \mathbf{r}'|) , \tag{3}$$

where $H_0^{(1)}$ is the zero-order Hankel function of the first kind and where $k = \omega/c$. The incident field is taken as a Gaussian tapered plane wave.[8] The scattered field at arbitrary points above the surface is then given by

$$H_s(\mathbf{r}) = \int_s \frac{\partial G_0(\mathbf{r}, \mathbf{r}')}{\partial n'} H(\mathbf{r}')\, ds' . \tag{4}$$

In scattering cross section calculations, the scattered field is needed in the far field, and a far field form of (4) is used. In order to obtain the scattered field close to the surface, however, the more general form given by (4) is used here.

If the metal is a good conductor, the magnetic field will penetrate into the conductor, and we must deal with the more general two-medium problem separated by a rough interface. The boundary conditions at the interface are that $H(\mathbf{r})$ and $(1/\varepsilon)[\partial H(\mathbf{r})/\partial n]$ are continuous; ε is the dielectric constant, which here is unity above the surface. The following coupled integral equations are obtained for $H(\mathbf{r})$ and its normal derivative

$$H(\mathbf{r}) = 2H_{\text{inc}}(\mathbf{r}) + 2\int_s \left[\frac{\partial G_0(\mathbf{r}, \mathbf{r}')}{\partial n'} H(\mathbf{r}') - G_0(\mathbf{r}, \mathbf{r}') \frac{\partial H(\mathbf{r}')}{\partial n'} \right] ds' \tag{5}$$

and

$$H(\mathbf{r}) = -2\int_S \left[\frac{\partial G_2(\mathbf{r},\mathbf{r}')}{\partial n'} H(\mathbf{r}') - \varepsilon_2 G_2(\mathbf{r},\mathbf{r}')\frac{\partial H(\mathbf{r}')}{\partial n'}\right] ds'. \tag{6}$$

In (6) ε_2 is the complex dielectric constant of the metal and

$$G_2(\mathbf{r},\mathbf{r}') = \frac{i}{4} H_0^{(1)}(k_2|\mathbf{r}-\mathbf{r}'|) \tag{7}$$

where $k_2 = \sqrt{\varepsilon_2}\,\omega/c$. Note that (6) requires the evaluation of Hankel functions of complex argument. After solving (5) and (6) for the surface fields, the scattered field in the vacuum above the surface is given by

$$H_s(\mathbf{r}) = \int_S \left[\frac{\partial G_0(\mathbf{r},\mathbf{r}')}{\partial n'} H(\mathbf{r}') - G_0(\mathbf{r},\mathbf{r}')\frac{\partial H(\mathbf{r}')}{\partial n'}\right] ds' . \tag{8}$$

The integral equation, (2), or the coupled integral equation system, (5) and (6), can be reduced to matrix equations and solved numerically following standard methods (see, for example Refs. 7 and 8). The solution of (2) gives $H(\mathbf{r})$ on the surface $z = f(x)$ at a set of N equally spaced points along the x-axis. For the examples to be discussed, we have used an x-axis partition interval $\Delta x = \lambda/10$, where λ is the wavelength in vacuum. Equations (4) and (8) then reduce to sums over these N points. Either (4) or (8) is used to obtain the scattered field at a rectangular array of field points close to the surface for display in color-coded plots.

Two important modifications were made to the general procedure just described. The first is necessary only for very good conductors of the type to be considered here, but the second is necessary for all cases.

Scattering from gold surfaces at a wavelength of 3.392 μm has been chosen to illustrate surface wave properties. Gold is a very good conductor for radiation of this wavelength, and yet, as we will see, the surface wave properties for gold are very different than those for a perfect conductor. The complex index of refraction for gold at 3.392 μm is $n = 1.958 + 20.7i$, and the corresponding complex dielectric constant is $\varepsilon_2 = -424.7 + 81.1i$. For such values of ε_2 it is not difficult to show that G_2 will vary significantly over Δx even when $\Delta x = \lambda/10$. Thus, the normal practice of approximating G_2 and its normal derivative as constant over each Δx when developing the matrix equations leads to significant error. Reducing Δx to $\lambda/40$ gives improved results; however, even finer partitioning appears necessary for this case, and the approach of refining the partitioning becomes computationally unwieldy. One approach that does work in evaluating the matrix elements is to approximate $H(\mathbf{r})$ and $\partial H(\mathbf{r})/\partial n$ in (6) as constant over Δx, and then to integrate the more rapidly varying quantities G_2 and $\partial G_2/\partial n$ numerically over Δx. This method has been developed and gives reliable results, but a simpler method to be described next gives essentially identical results and therefore has been used for the examples to be discussed.

The conductivity of gold at 3.392 μm is sufficiently high that $H(\mathbf{r})$ and its normal derivative are very accurately related by an impedance condition

$$\frac{\partial H(\mathbf{r})}{\partial n} = kH(\mathbf{r}) \Big/ \sqrt{-\varepsilon_2} \,. \tag{9}$$

The impedance condition (9) is just the first term in an expansion in powers of skin depth,[9] but it is entirely adequate for the present case. Use of (9) in (5) leads to a single integral equation for $H(\mathbf{r})$, and (6) is not used. Thus, the matrix size for our system of equations is reduced from $2N \times 2N$ to $N \times N$, which yields a major reduction in computation time. In addition, only Hankel functions of real arguments are required, which is an added benefit. After $H(\mathbf{r})$ is obtained from (5), the scattered field is found with (8), again using (9). Comparisons between the solutions obtained using the full coupled equation system of (5) and (6) and using the impedance condition (9) in (5) show essentially perfect agreement for gold at 3.392 μm. Therefore, the impedance method was used for the good conductor cases to be discussed. For other metals or frequencies, such agreement would need to be reconfirmed, and an improved impedance approximation or the full solution method may well be necessary.

The second modification to the general procedure for calculating the scattered field is made only for field points very close to the surface. Typically, (4) or (8) is used to find $H_s(\mathbf{r})$ in a rectangular array of field points with horizontal and vertical spacings of $\lambda/10$. The procedure as described works well except for field points that happen to be within a small fraction of a wavelength from one of the set of N points that define the rough surface. The field is compute on a prescribed set of points independent of the rough surface profile, and when a field point is very close to a surface point, the approximation of replacing (4) or (8) as a simple sum becomes inaccurate. The rapid variation of G_0 as $\mathbf{r}'$ passes close to $\mathbf{r}$ must be taken into account in the integration to obtain accurate results.

The modified procedure is as follows. The medium in which each field point resides is determined assuming that straight lines connect the N points defining the surface. If the field point lies inside the metal, the field is not computed, and the color set to black. For the good conductor case, the actual field can be found using an expression analogous to (8) that is valid in the second medium. However, for gold the field drops off very rapidly with increased depth in the metal, and for simplicity this field has not been included. Next, the field point is tested for closeness to surface points. Whenever $k|\mathbf{r} - \mathbf{r}'| < 0.9$, the corresponding term in (4) or (8) is replaced by an analytic integration over Δx. This is done by making a small argument expansion of $H_0^{(1)}$ and keeping terms up to the argument-squared term (the first four terms). The integration over Δx can then be done analytically, taking the normal derivative of $H(\mathbf{r})$ as constant over this interval. Similarly, the normal derivative of G_0 yields $H_1^{(1)}$ which is also expanded in a small argument series with terms kept up to the argument squared term (the first five terms). Again, an analytic integration is done over Δx. The result of this modification is to produce a smooth scattered field right up to the surface, including the regions within the corrugations of the rough surface.

2.2 Examples of field visualization in p-polarized scattering

Examples of fields near rough surfaces for good and perfect conductors are shown in Figs. 1–3. These color field maps were made by first contouring the field values that were computed as described in Section 2.1 and then assigning colors to the field values on a linear scale. For the examples shown, the surface was modeled with a Gaussian surface height spectrum with $kh = 0.1$ or 0.5 and $kl = 1.0$, where k is the radiation wavenumber, h is the rms surface height, and l is the $1/e$ correlation length. The rough surface extends from –450 to +450 on the horizontal axis, and a wavelength equals ten units. The incident field is a Gaussian tapered plane wave centered at zero on the horizontal scale and with an incident angle of 45°. The $1/e$ points for the incident field are at ±100 on the horizontal scale, and here we display the scattered field well away from the region where the incident field has significant magnitude.

For $kh = 0.1$ most of the energy in the scattered field resides in the coherent component, which propagates in the specular direction. The smaller incoherent field scatters in all directions. It turns out that for $kl = 1.0$, and with the boundary conditions under study, more incoherent energy is scattered in the back direction than the forward direction. (For $kl = 2.0$, there is about equal backward and forward scattering, and as kl is increased further forward scattering dominates.) Therefore we display fields near the surface in the back direction to look for surface waves; the fields in the forward direction are similar but with somewhat reduced magnitude.

Figure 1 shows the magnitude of the scattered field for a perfect conductor (a) and a good conductor (b) for the same surface realization ($kh = 0.1$). The roughness of the surface is too small to be seen for this case, and as mentioned in Section 2.1 only the field on the vacuum side of the interface is shown. In the initial integral equation calculation of the surface field, the rough surface continues on to the left to –450 to avoid edge effects in the field maps shown. Numerical studies show that extending the surface endpoint farther to the left makes no significant difference. The incident field has not been added to the scattered field to yield the total field and thus is not included. In any case, the incident field would be almost entirely out of the field of view; it propagates from the upper left to the lower right and is concentrated either above or to the right of the view shown. Thus, the figures display the near-surface region to the left of where the main part of the incident field illuminates the surface. The range on the magnitude scale is from 0.0 to 0.25, while the magnitude of the incident field is 1.0 at 0.0 on the horizontal scale.

In Fig. 1 the large feature in the middle to upper part of both (a) and (b) is a lobe of freely propagating scattered energy moving up and to the left. This structure depends on the particular surface realization used and would differ for each realization. Note that this lobe is similar for the good and perfect conductor models. In fact, evaluation of the scattered field in the far field of the surface yields results that are very close for both models. However, the structure near the surface is very different for these two cases, and this difference can have important consequences for theoretical treatments of scattering.

A surface wave should appear as an enhancement of the field near the surface. In Fig. 1 the good conductor shows a clear surface wave, while the presence of a surface wave is not evident for the perfect conductor. Note also that the field magnitude in the surface wave shows a clear modulation with a half-wavelength period (five units). Numerical studies show this to be a standing wave pattern set up by right- and left-propagating surface waves. Though a predominantly

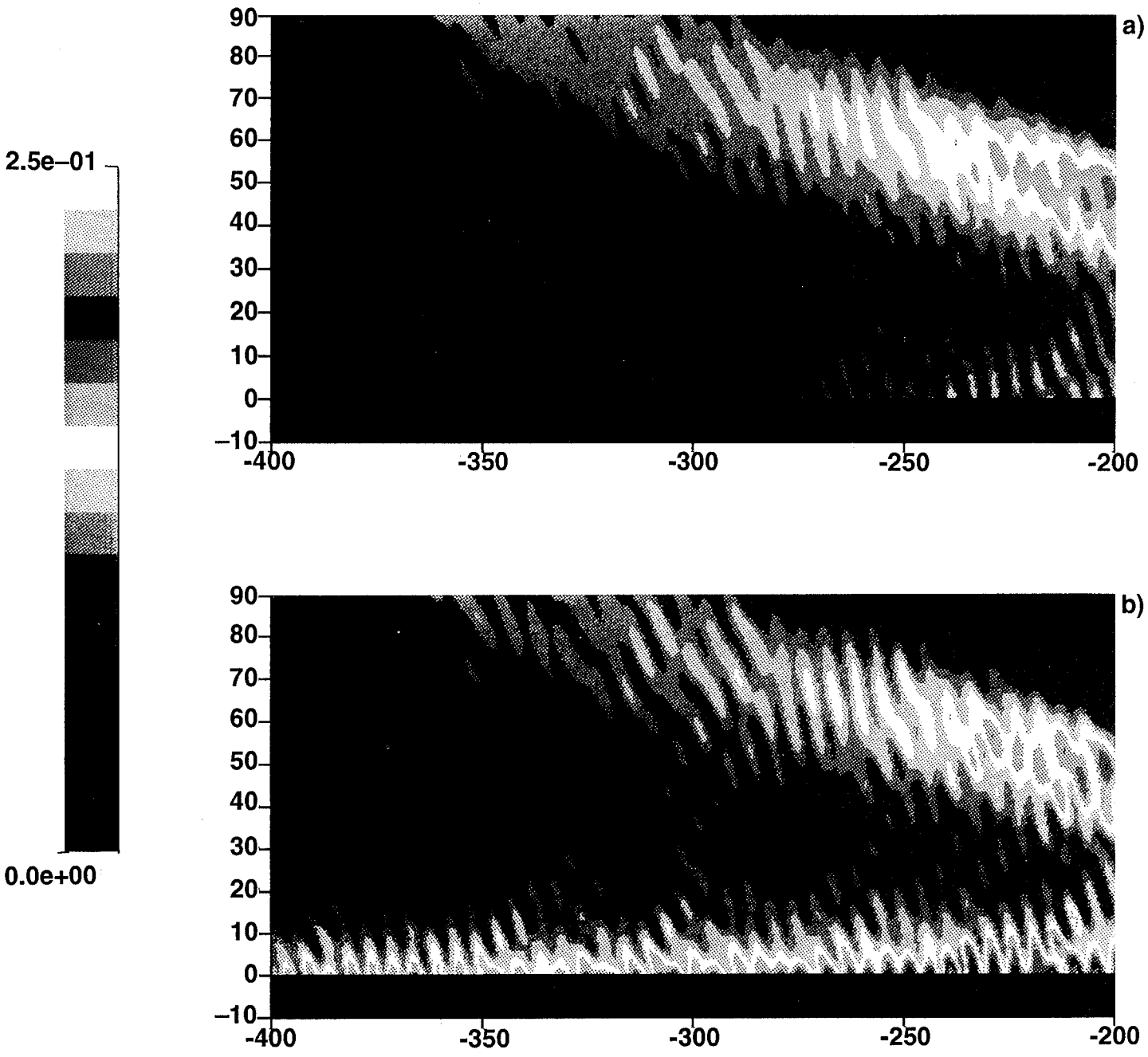

Figure 1. Backscattered field magnitude near rough surface with kh = 0.1 and kl = 1.0: (a) perfect conductor, (b) good conductor. The view is to the left of the region directly illuminated with a tapered plane wave incident field (θ_i = 45°), which is centered at zero on the horizontal scale. A radiation wavelength equals ten units, and the color scale is linear in the field magnitude.

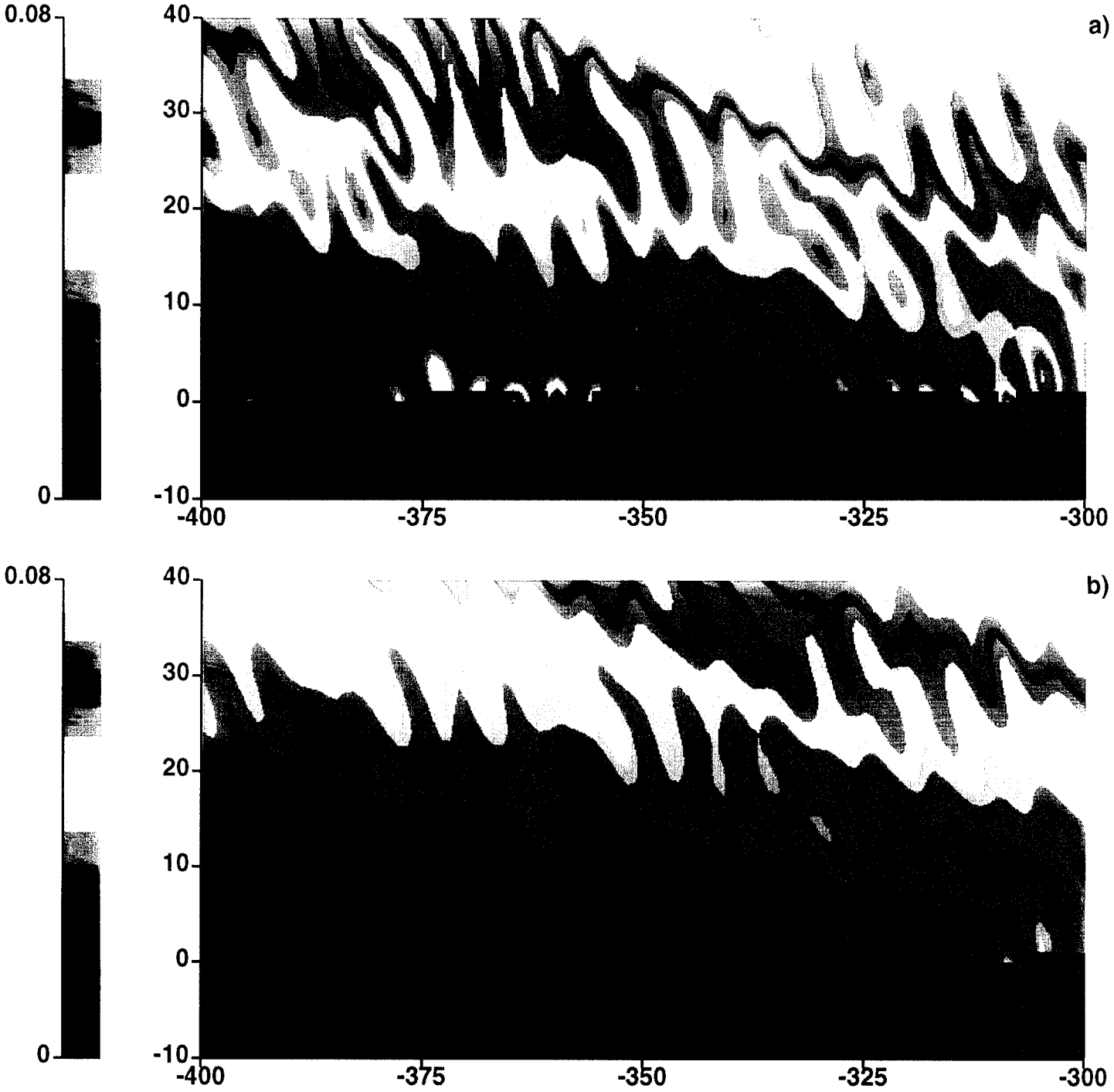

Figure 2. Field magnitude with kh = 0.5 and kl = 1.0: (a) perfect conductor, (b) good conductor. The true shape of the rough surface profile is not accurately represented in the display.

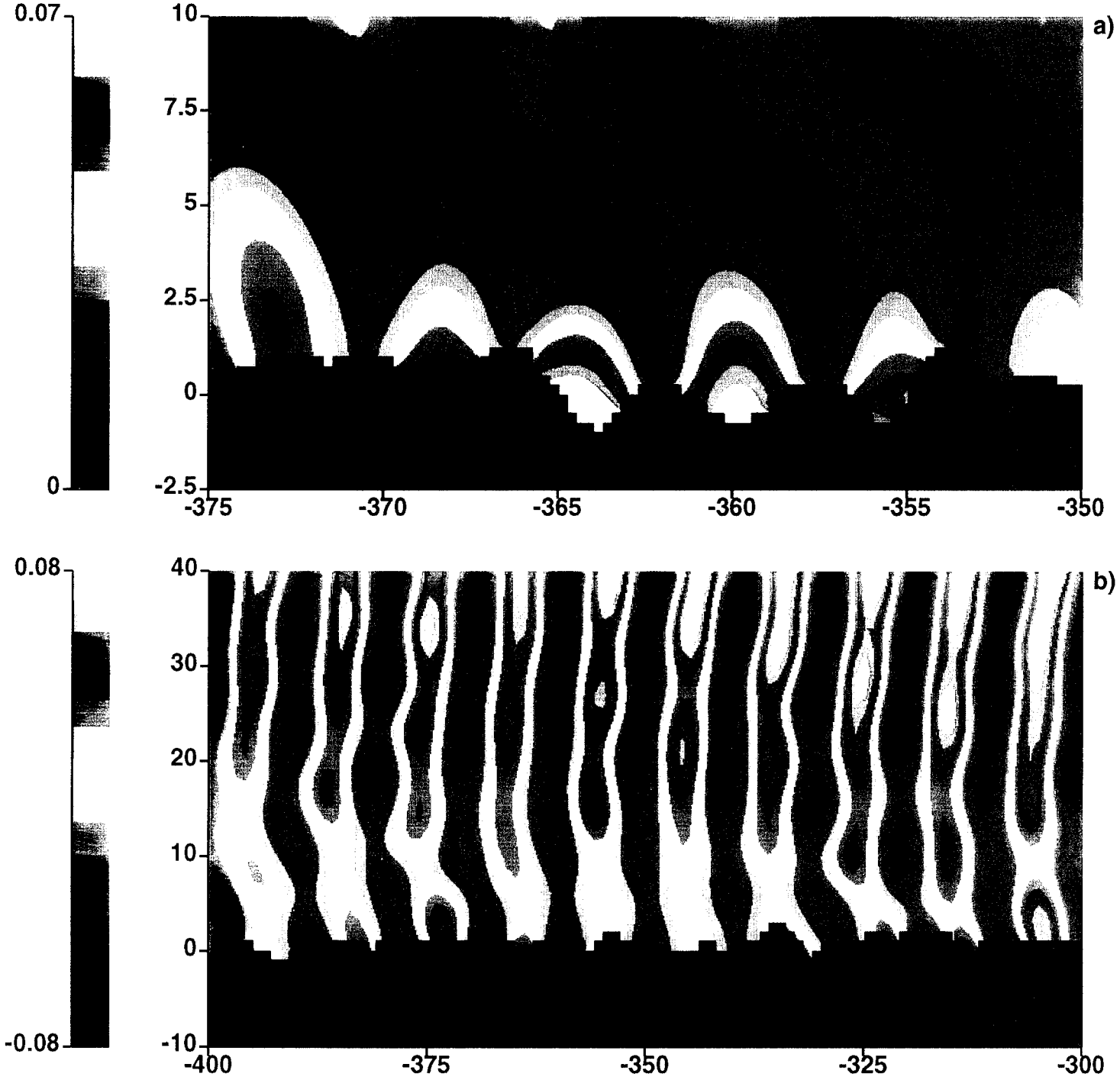

Figure 3. Fields for a perfect conductor: (a) blowup of part of Fig. 2(a) showing field magnitude close to surface. Note color scale has been changed slightly from Fig. 2(a). (b) The real part of the field corresponding to Fig. 2(a).

left-propagating surface wave might be expected for the geometry of Fig. 1, the roughness is sufficient to generate a right-going wave as well. If the surface is set flat to the left of −300, for example, the modulation vanishes to the left of that point and grows rapidly to the right of that point. The modulation period remains at one half wavelength when kl is increased to 2.0, showing that the scale length of the roughness does not determine the modulation period. Analytic estimates show that when an evanescent wave interacts once with the rough surface with $kl = 1.0$, there is a greater amplitude (or, more precisely, a greater transition matrix element) for scattering into back-traveling evanescent waves than into forward-traveling evanescent waves. This occurs for essentially the same reason that the far field backscattering level is higher than the forward scattering level. The dominance of backscattering apparently leads to the establishment of the standing wave pattern. When kl is increased to 3 or 4, the amplitude for scattering into forward-traveling waves, freely propagating or evanescent, is much greater than the amplitude for scattering into backward traveling waves. In this case, surface waves are still produced for the good conductor (now looking in the forward region, e.g., from +200 to +400), but the half-wavelength modulation is absent.

As mentioned, the perfect conductor does not show a clear surface wave in Fig. 1(a), but on close inspection there is some evidence for one. There is half-wavelength modulation of the field near the surface (and extending well above it), and there is some weak enhancement of the field near the surface. By studying a series of cases with increasing kh, one can see more clearly that a surface wave does exist in the perfect conductor case, though it is weak when $kh = 0.1$ and not particularly convincing from Fig. 1(a) alone.

Figure 2 compares field magnitudes for perfect [Fig. 2(a)] and good [Fig. 2(b)] conductors when kh is increased to 0.5 with kl and the incident angle unchanged. Note that the view here is in closer to the surface, showing half as much surface length. The roughness of the surface can now be seen, but the "blocky" appearance of the interface is an artifact of the plotting process and does not accurately represent the rough interface profile. (The potential problem here is that the contouring routine can produce a blurred interface. To avoid this, the "field magnitude" has been set to −100 when the field point lies in the metal. The contouring routine then creates a sharp boundary along edges of the 1 unit × 1 unit cells used to sample the field. A more accurate representation of the interface can be obtained by reducing this cell size, but a smaller grid is not necessary to represent the field itself accurately.)

For the case shown in Fig. 2, the roughness is higher than for Fig. 1, and consequently more energy is scattered in the back direction. Because some energy is lost in the metal for the good conductor (resistive loss), the levels are lower. Note that the field propagating at low scattered grazing angles, that is, nearly parallel to the surface, is much reduced in magnitude. Apparently, the field components propagating at low grazing angles close to the surface have a high probability of rescattering from the rough surface to higher grazing angles. The field propagating close to the surface is therefore effectively stripped away.

It is also evident in Fig. 2 that there is field enhancement close to the surface (within about five units, or one-half wavelength), and hence a surface wave is present, though it decays more rapidly with distance along the surface. For this case, the surface wave field structure is similar for

the good and perfect conductor models. Again, a modulation of the surface wave magnitude can be observed at a one-half-wavelength period. The modulation is more clear in the close-up view for the perfect conductor shown in Fig. 3(a). The field structure gives the appearance of bound modes that are enhanced when they coincide with cavities in the surface profile. The surface wave field structure for the good conductor is similar, except it is reduced in level somewhat by losses in the metal. In Fig. 3(a) the field magnitude was computed on a 0.2×0.2 unit grid, giving a better representation of the surface profile.

We see that when $kh = 0.5$ and $kl = 1.0$ the roughness alone is sufficient to support a surface wave, as shown by the perfect conductor results. For the good conductor model, the complex dielectric constant of the metal is of secondary importance in determining the surface wave properties, because in this case the rough surface scattering losses are evidently more important than resistive losses for surface wave attenuation. As a consequence, the surface wave properties of the perfect and good conductor models are similar. In contrast, when $kh = 0.1$ and $kl = 1.0$, the roughness alone can support only a weak surface wave. Scattering losses are also much reduced, and a relatively strong surface wave can be produced on the good conductor, supported by the complex dielectric properties of the metal.

Finally, another interesting phenomenon is shown in Fig. 3(b). This figure shows the real part of the field for the perfect conductor, corresponding to Fig. 2(a). The color scale now includes negative and positive values, and the zero level is in the green region. The real part of the field shows the phase fronts, which are advancing to the left. The interesting feature here is the presence of a phase lag right near the surface which occurs when the roughness is relatively large. When $kh = 0.1$, the phase fronts come smoothly down to the surface, showing no phase lag. This is an example of a phenomenon that can be readily examined with field visualization, but may be more difficult to study with more traditional theoretical and numerical methods.

In summary, field visualization can be a very useful method for gaining physical insight into complex scattering phenomena and should prove to be a valuable supplement to theoretical investigations of electromagnetic scattering.

3. Perturbation Theory for the Neumann Boundary Condition

The presence of surface waves is related to difficulties that occur with theoretical treatments of p-polarized scattering from rough surfaces. The general area of interest here is scattering from conducting surfaces with roughness that is small in comparison with the radiation wavelength. This is the regime where perturbation theory is usually assumed to apply. However, it is not completely straightforward to develop and apply perturbation theory to these scattering problems, because of the possible excitation of surface electromagnetic waves. The difficulty appears most acutely for p-polarized scattering from a rough, perfectly conducting surface (the Neumann boundary condition), which for simplicity we consider to be a one-dimensional (1-D) surface. For p-polarized scattering, the electric vector is in the plane of incidence. In the standard perturbation method, the scattering problem is solved using a consistent expansion in the small parameter kh, where k is the radiation wavenumber and h is the rms surface height of the roughness. When this approach is applied to p-polarized scattering from perfect conductors, the lowest-order result is

incorrect near grazing, and divergences appear[4,5] beyond lowest order. The existence of surface electromagnetic waves leads to a breakdown in the standard perturbation approach: Many of the higher-order perturbation theory terms are not negligibly small, even when $kh << 1$. A correct theoretical treatment for this problem requires a partial summation of these higher order terms;[2,5] that is, a renormalization procedure is required. (A large literature exists on theoretical treatments of this problem, and no attempt will be made here to be complete.) Because of the need for renormalization, the complexity of perturbation theory is significantly increased for this problem, and numerical evaluations are much more difficult.

For this project, we have specialized to the perfect conductor case. The goal has been to develop a perturbation theory capable of giving accurate results for kh up to 0.5. Perturbation theory, if taken beyond lowest order, is valid for s-polarized scattering from perfect conductors (Dirichlet boundary condition) up to about this level of roughness.[6] However, renormalization is not necessary for s-polarized scattering. The goal here is to reach approximately the same level of accuracy for the Neumann problem where renormalization is required. The results to be presented show that this goal has been essentially reached.

Fortunately, the fundamental renormalized perturbation theory for electromagnetic scattering from rough surfaces has been elegantly worked out by Maradudin and co-workers.[2-5] However, because of the complexity of the results for the scattering cross section, simplifying approximations have been used when doing numerical calculations. First, attention has focused on cases with $kh << 1$, which allows a less rigorous evaluation. Second, the pole approximation has often been used for the Green's function for surface electromagnetic waves, again simplifying the evaluation. What distinguishes the present approach is that a full numerical implementation of the renormalized perturbation theory is made, without approximation beyond the basic perturbation approximation (with renormalization). The most challenging part of this program is the solution of a nonlinear integral equation for the "self-energy" (also known as the mass operator). A rigorous evaluation of this quantity turns out to be necessary to obtain accurate results for kh up to 0.5. Previous work by others has relied on more approximate evaluations of this quantity.

In Section 3.1 a summary of the theoretical results for the scattering cross section and the self-energy (or mass operator) will be given, together with an outline of the method used for numerical evaluation. A consistency condition known as the Ward identity will also be discussed. In Section 3.2, the accuracy of renormalized perturbation theory for the perfect conductor case will be shown through comparisons with exact integral equation results.

3.1 Analytical results from perturbation theory

We specialize to scattering from a one-dimensional (1-D) surface subject to the Neumann boundary condition (p-polarized scattering from a perfect conductor). The strength of the scattering will be characterized in terms of the bistatic scattering cross section[6] σ. When the incident and scattering angles are measured relative to the vertical axis in the usual fashion, then σ is related to the differential reflection coefficient $\partial R/\partial\theta_s$, also commonly used,[7] by

$$\sigma = \cos\theta_i \langle \frac{\partial R}{\partial \theta_s} \rangle, \tag{10}$$

where θ_i is the angle of incidence and $< >$ denotes an ensemble average. The plane of incidence is the x-z plane, and the rough surface profile is defined by $z = f(x)$, where the mean surface height is zero and where the z axis is directed upward from the metal into a vacuum. We denote the radiation wavenumber by k, where $k = \omega/c$. Horizontal components of wave vectors will be denoted by k with a subscript. In particular, the horizontal components of the incident and scattered wave vectors are k_i and k_s, respectively. Expressions will be given first for standard perturbation theory, followed by those for renormalized perturbation theory.

3.1.1 Standard perturbation theory

For standard perturbation theory, the lowest-order result for the scattering cross section is given by

$$\sigma_s^{11} = \frac{4}{k} u^2(k_i, k_s)\, W(k_s - k_i). \tag{11}$$

At lowest order, the field is found to first order in kh; thus, the scattered intensity and the scattering cross section are to second order in kh. This is denoted by the 11 superscript on σ, and the subscript s simply indicates standard perturbation theory. Also in (11),

$$u(k_1, k_2) = k^2 - k_1 k_2 \tag{12}$$

and $W(K)$ is a Gaussian roughness spectrum given by

$$W(K) = \frac{1}{2\pi} \int_{-\infty}^{\infty} dx\, \rho(x)\, e^{-iKx} = \frac{lh^2}{2\sqrt{\pi}} e^{-K^2 l^2/4}, \tag{13}$$

where $\rho(x)$ is the surface correlation function:

$$\rho(x) = \langle f(x_1)\, f(x_1 + x) \rangle = h^2 e^{-x^2/l^2}. \tag{14}$$

The form given by (11) does not vanish as θ_i or θ_s approach grazing, though it is possible to argue from quite general grounds that σ must have this property. This indicates that (11) must be inaccurate close to grazing.

In order to obtain an expression for the scattering cross section that is accurate for greater values of kh than (11), it is logical to carry perturbation theory to higher order. When the field is found to second order in kh, we obtain a contribution to the cross section that is fourth order in kh, which we denote σ_s^{22}. (Another term at fourth order, σ_s^{13}, is obtained from a product of first- and third-order contributions to the field, but this term will not be discussed in the context of standard perturbation theory.) The result is

$$\sigma_s^{22} = \frac{4}{k} \int_{-\infty}^{\infty} dk_1\, W(k_s - k_1)\, W(k_1 - k_i)\, u(k_s, k_1)\, u(k_1, k_i)\, (J_1^{[0]} + J_2^{[0]}), \tag{15}$$

where

$$J_1^{[0]} = u(k_s, k_1)\, u(k_1, k_i) \left| G^{[0]}(k_1) \right|^2 \tag{16}$$

and

$$J_2^{[0]} = u(k_s, k_i + k_s - k_1)\, u(k_i + k_s - k_1, k_i)\, G^{[0]}(k_1)\, G^{[0]*}(k_i + k_s - k_1), \tag{17}$$

where * denotes complex conjugation. In these expressions, the Green's function

$$G^{[0]}(k_1) = \frac{i}{\alpha_0(k_1)}\ , \tag{18}$$

where

$$\alpha_0(k_1) = \begin{cases} \left(k^2 - k_1^2\right)^{1/2} & k_1^2 < k^2 \\ i\left(k_1^2 - k^2\right)^{1/2} & k_1^2 > k^2 \end{cases}\ . \tag{19}$$

As noted previously,[1,5] the factor in (16) given by $|G^{[0]}(k_1)|^2 = |k^2 - k_1{}^2|^{-1}$ causes the integral in (15) to diverge. Similarly, $J_2^{[0]}$ gives a divergence for backscatter ($k_s = -k_i$). Clearly, fundamental problems exist with standard perturbation theory, and a different method is needed.

3.1.2 Renormalized perturbation theory

Renormalized (or self-energy) perturbation theory is developed and discussed for scattering from general media in Refs. 2–4 and specialized to the 1-D Neumann rough surface in Ref. 5. A renormalized version of σ^{11} is given in Ref. 5, and renormalized expressions for σ^{22} and σ^{13} can be obtained from the general theory presented there. This is accomplished by iteration of the Bethe-Salpeter equation, which is given by Eq. (6.1) in Ref. 5. Only the results will be given here. It should be mentioned that the meaning of the σ superscripts is different for renormalized perturbation theory than for standard perturbation theory. Since a partial summation of higher-order terms has been accomplished in the renormalization, contributions to all orders of kh are present in each term of the renormalized perturbation series. Nevertheless, there is a natural way of designating a new series of terms, which corresponds term by term with the standard perturbation series; thus, the same superscript notation is used.

The lowest-order expression for the bistatic scattering cross section obtained with renormalized perturbation theory is given by

$$\sigma^{11} = \frac{4k_{iz}^2 k_{sz}^2}{k} u^2(k_i, k_s) \left| G^{[2]}(k_i) \right|^2 \left| G^{[2]}(k_s) \right|^2 W(k_s - k_i), \tag{20}$$

where $k_{iz} = -\alpha_0(k_i)$, $k_{sz} = \alpha_0(k_s)$, and

$$G^{[2]}(k_1) = \frac{i}{\alpha_0(k_1) - iM^{(2)}(k_1)}, \tag{21}$$

where $G^{[2]}(k_1)$ is an approximation to the surface electromagnetic Green's function $G(k_1)$, and where $M^{(2)}(k_1)$ is an approximation to the self-energy (or mass operator) $M(k_1)$. (If the superscripts are removed in (21), the proper relation connecting $G(k_1)$ and $M(k_1)$ is obtained.) In the approximation being considered presently, the self-energy is given by

$$M^{(2)}(k_1) = \int_{-\infty}^{\infty} dk_2 \, u^2(k_1, k_2) \, G^{[2]}(k_2) \, W(k_1 - k_2). \tag{22}$$

Using (21) in (22) gives a nonlinear integral equation for $M^{(2)}(k_1)$. The renormalization of the theory leads to the presence of $M^{(2)}(k_1)$ in (21), and it is not difficult to see that if $M^{(2)}(k_1)$ is set to zero, (20) reduces to the standard perturbation theory result given by (11). Note also that the factors $k_{iz}^2 k_{sz}^2$ in (20) lead to acceptable behavior of σ^{11} near grazing.

The full self-energy $M(k_1)$ satisfies an integral equation,[1,5] and approximations to $M(k_1)$ are obtained by iteration, with $M^{(2)}(k_1)$ being the lowest-order term. The superscript here indicates that, aside from the Green's function which contains all orders of kh, the approximation to the self-energy in (22) is of second order in kh. Though (22) is the lowest-order approximation to $M(k_1)$ obtained by iteration, it is still complicated to evaluate because a nonlinear integral equation must be solved. Because of this complexity, the expression for $M^{(2)}(\mathrm{k}_1)$ has apparently always previously been further approximated by replacing $G^{[2]}(k_1)$ with $G^{[0]}(k_1)$, which reduces (22) to an integral. The approximation used for $M(k_1)$ determines the extent of the processes that are included in the renormalization scheme, and it is not clear from theoretical considerations alone what level of approximation is required. Some insight can be gained by displaying the processes that enter using Feynman diagrams,[2] but that will not be discussed here. We found by numerical evaluation that the further approximation to $M^{(2)}(k_1)$ just mentioned was not adequate for the relatively large values of kh of interest here. Thus, we have used (22) as it stands, which evidently has not been done previously.

There is also a consistency condition known as the Ward identity[2] that involves $M(k_1)$ and quantities that enter into the scattering cross section series. This will be discussed shortly, but it can be mentioned here that (20)–(22) are consistent with this condition. To obtain a renormalized perturbation theory for the Neumann boundary condition that is accurate up to $kh = 0.5$, it is necessary to extend the series beyond the σ^{11} term to the σ^{22} and σ^{13} terms. We first consider this extension without improving the approximation to $M(k_1)$, which would be required to remain consistent with the Ward identity.

The renormalized results for σ^{22} and σ^{13} are as follows

$$\sigma^{22} = \frac{4k_{iz}^2 k_{sz}^2}{k}\left|G^{[2]}(k_i)\right|^2\left|G^{[2]}(k_s)\right|^2 I_1 \,, \tag{23}$$

$$I_1 = \int_{-\infty}^{\infty} dk_1 W(k_s - k_1)\, W(k_1 - k_i)\, u(k_s, k_1)\, u(k_1, k_i)\, (J_1^{[2]} + J_2^{[2]}) \,, \tag{24}$$

$$J_1^{[2]} = u(k_s, k_1)\, u(k_1, k_i)\left|G^{[2]}(k_1)\right|^2, \tag{25}$$

$$J_2^{[2]} = u(k_s, k_i + k_s - k_1)\, u(k_i + k_s - k_1, k_i)\, G^{[2]}(k_1)\, G^{[2]*}(k_i + k_s - k_1) \,, \tag{26}$$

$$\sigma^{13} = \frac{4k_{iz}^2 k_{sz}^2}{k} u(k_i, k_s)\left|G^{[2]}(k_i)\right|^2\left|G^{[2]}(k_s)\right|^2 W(k_s - k_i)\left[-2\mathrm{Re}\,(I_2) + I_3\right], \tag{27}$$

$$I_2 = \int_{-\infty}^{\infty} dk_1 u(k_s, k_s - k_1)\, u(k_s - k_1, k_i - k_1)\, u(k_i - k_1, k_i) \times G^{[2]}(k_i - k_1)\, G^{[2]}(k_s - k_1)\, W(k_1), \tag{28}$$

and

$$I_3 = \left[2k^2 - (k_i + k_s)^2 + \frac{k_i k_s\left(k_i^2 + k_s^2\right)}{k^2} + \frac{4k_i k_s}{(kl)^2}\right](kh)^2. \tag{29}$$

Comparison of (23)–(26) with (15)–(17) shows that σ^{22} reduces to $\sigma_s{}^{22}$ when $M^{(2)}(k_1)$ is set to zero, and a similar reduction occurs for σ^{13}. All expressions through (28) are valid for general spectral density functions for the surface roughness, assuming the surface statistics are Gaussian. The last term in (29), however, is specialized to a Gaussian spectrum. More generally, this term involves an integration over $k_1{}^2 W(k_1)$, which can be expressed in terms of the mean square slope of the surface. In (29) a Gaussian spectrum was assumed for expressing the mean square slope.

3.1.3 Evaluation of renormalized perturbation theory

The principal challenge in evaluating (20), (23), and (27) is to obtain the self-energy $M^{(2)}(k_1)$. Once that is done, the remaining calculation is straightforward. The natural approach to solving the nonlinear integral equation (22) is to use iteration, assuming $M^{(2)}(k_1)$ is small. Taking this tack, one would initially set $M^{(2)}(k_1)$ in $G^{[2]}(k_1)$ to zero and iterate (22). Unfortunately, this method does not lead to convergence to a solution for large $|k_1|$ and does not give the correct scattering cross section, except for small kh. The problem is that $M^{(2)}(k_1)$ is not uniformly small, but instead grows quadratically with k_1 for large $|k_1|$. As kh increases, it becomes increasingly important to compute $M^{(2)}(k_1)$ accurately in this asymptotic region. It is not difficult to show from (22) that for very large $|k_1|$, the leading-order solution for $|M^{(2)}(k_1)|$ is $k_1{}^2 h$. It also follows from (21)

and (22), that $M^{(2)}(k_1)$ must be an even function of k_1. Thus, using a descending polynomial form in $|k_1|$ beginning at the $k_1{}^2$ term, we find from (22) the following asymptotic solution:

$$M_0^{(2)}(k_1) = ik_1^2 h + \frac{1}{2}|k_1| - i\left(k^2 h + \frac{1}{8h}\right) - \frac{k^2}{4|k_1|}\left[1 - \frac{2}{(kl)^2}\right]. \tag{30}$$

Only the last term involving kl depends on the spectral density function being Gaussian. All other terms are valid for arbitrary $W(K)$. Equation (30) is valid for large $|k_1|/k$ but not for small $|k_1|/k$. We found that an adequate initial solution for $M^{(2)}(k_1)$ is given by (30) when $\mathrm{Im}[M_0{}^{(2)}(k_1)] > 0$ and zero otherwise. The solution for $M^{(2)}(k_1)$ is then found by repeated iteration of (22).

For the purpose of iteration and for later use in (20), (23), and (27), it is convenient to represent $M^{(2)}(k_1)$ as a piecewise continuous function. This was done by selecting a finite range of k_1 determined by $|k_1| < k_0$ over which $M^{(2)}(k_1)$ is to be determined. This range was selected so that for larger $|k_1|$ the asymptotic solution given by (30) is adequate. (Typically, $k_0 = 7k$.) The region $|k_1| < k_0$ was then divided into several intervals, and on each interval values for the real and imaginary parts of $M^{(2)}(k_1)$, computed from (22) with the initial solution used in (21), were fitted by 40th-order Chebyshev polynomials. This piecewise continuous representation for $M^{(2)}(k_1)$, which includes the asymptotic solution for $|k_1| > k_0$, was then used in (22) to obtain updated values for $M^{(2)}(k_1)$, which were again fitted with Chebyshev polynomials. The iteration process was then repeated, and convergence to machine precision was obtained in about ten iterations. The final piecewise continuous representation of $M^{(2)}(k_1)$ was then used in (20), (23), and (27).

3.1.4 The Ward identity

When there is no resistive energy loss (as is the case for the perfect conductor), the Ward identity[2] is a relation that connects the self-energy $M(k_1)$ with another quantity called the averaged irreducible vertex function.[2,5] Energy conservation will be ensured in a given approximation if the Ward identity is satisfied. The irreducible vertex function satisfies an integral equation and enters into the Bethe-Salpeter equation, also an integral equation. Both of these integral equations are iterated in generating the renormalized perturbation series for the scattering cross section. The Ward identity, then, is a consistency condition between the approximation used for $M(k_1)$ and the terms included in the scattering cross section series. It is not clear *a priori* how important it is to satisfy the Ward identity in order to obtain an accurate approximation to the scattering cross section.

The Ward identity is given by[2]

$$\mathrm{Im}\,[M(k_1)] = \int_{-\infty}^{\infty} \frac{dk_2}{2\pi} \mathrm{Im}\,[G(k_2)\,U(k_2, k_1)] \tag{31}$$

where $U(k_2, k_1)$ is the averaged irreducible vertex function. For σ^{11} we need only the lowest-order result for $U(k_2, k_1)$ given by

$$U^{(2)}(k_2, k_1) = 2\pi u^2(k_1, k_2)\, W(k_1 - k_2)\,. \tag{32}$$

With the lowest-order expressions for $U(k_2, k_1)$ and $M(k_1)$, the Ward identity becomes

$$\mathrm{Im}\left[M^{(2)}(k_1)\right] = \int_{-\infty}^{\infty} \frac{dk_2}{2\pi} u^2(k_1, k_2)\, W(k_1 - k_2)\, \mathrm{Im}\left[G^{[2]}(k_2)\right]. \tag{33}$$

It follows from (22) that the Ward identity is indeed satisfied for this case. It is therefore consistent with the Ward identity to use (22) for the self-energy when computing σ^{11}. When the perturbation series for the scattering cross section is extended to the σ^{22} and σ^{13} terms, however, the use of (22) is no longer sufficient to ensure satisfaction of the Ward identity, because a higher-order result is used for $U(k_2, k_1)$. Because of the complexity of computing $M(k_1)$ to higher order, we have at first continued to use $M^{(2)}(k_1)$ for σ^{22} and σ^{13} as indicated in (23)–(28). Results showing the accuracy of renormalized perturbation theory when using this approximation will be given in the next section. In addition, to examine the possible benefit of maintaining the consistency between $U(k_2, k_1)$ and $M(k_1)$, the self-energy has also been extended to the next order, as described next.

When $U(k_2, k_1)$ is computed for the cross section terms σ^{22} and σ^{13}, all terms to fourth order in kh are retained, again where only contributions apart from the Green's functions are counted. (This convention on order number will be assumed henceforth, and further reference to excluding the Green's functions will be omitted.) We therefore iterate the governing equation for $M(k_1)$ and keep all terms to the fourth order. The result is written in the following form

$$M^{[4]}(k_1) = M_4^{(2)}(k_1) + M^{(4)}(k_1) \tag{34}$$

where $M_4^{(2)}(k_1)$ is the second order part and is given by (22), except $G^{[2]}(k_1)$ is upgraded to $G^{[4]}(k_1)$, to be defined shortly. The superscript convention is that (n) indicates a term of nth order in kh, while $[n]$ indicates that all terms up to nth order are included. The fourth order term in (34) is given by

$$M^{(4)}(k_1) = \int dk_2 G^{[4]}(k_2)\, u(k_1, k_2)\, W(k_1 - k_2) \left[I(k_1, k_2) + V^{13}(k_1, k_2)\right], \tag{35}$$

where

$$\begin{aligned} I(k_1, k_2) = {} & \int dk_3 u(k_1, k_1 + k_3)\, u(k_1 + k_3, k_3 + k_2)\, u(k_3 + k_2, k_2) \\ & \times G^{[4]}(k_1 + k_3)\, G^{[4]}(k_3 + k_2)\, W(k_3) \end{aligned} \tag{36}$$

and

$$V^{13}(k_1, k_2) = (kh)^2 \left[2k^2 - (k_1 + k_2)^2 + k_1 k_2 (k_1^2 + k_2^2)/k^2 + 4k_1 k_2/(kl)^2\right]. \tag{37}$$

In these equations the Green's function $G^{[4]}(k_1)$ is given by

$$G^{[4]}(k_1) = \frac{i}{\alpha_0(k_1) - iM^{[4]}(k_1)}. \tag{38}$$

The Green's function superscript indicates the order of the self-energy that is in the denominator, and the square bracket is used because all contributions up to the highest are included in the self-energy. It can be shown that the Ward identity (31) is satisfied when $M^{[4]}(k_1)$, $G^{[4]}(k_1)$, and the corresponding $U^{[4]}(k_2, k_1)$ are used.

The computation of $M^{[4]}(k_1)$ proceeds along the same lines as described for $M^{[2]}(k_1)$ and will not be discussed in detail. An asymptotic form for $M^{[4]}(k_1)$ is used in (38) to begin the iteration of (34)–(38) in conjunction with (22), which is modified to give $M_4^{(2)}(k_1)$ as mentioned. After the solution for $M^{[4]}(k_1)$ is obtained, (20), (23), and (27) are evaluated with $G^{[2]}(k_1)$ everywhere replaced by $G^{[4]}(k_1)$. Note that in computing σ^{22} and σ^{13} such that the Ward identity is satisfied, the computation of σ^{11} is also modified.

3.2 Numerical results from perturbation theory

In this section comparisons with integral equation results are used to examine the accuracy of the various perturbation theory approximations discussed in Section 3.1. All examples assume p-polarized scattering from perfect conductors, i.e., the Neumann boundary condition. The surface roughness is described by a Gaussian roughness spectrum with $kl = 2.0$, and kh is varied. The angle of incidence is 45° for all examples. The integral equation scattering cross sections were obtained by averaging the results for 50 surface realizations, and a tapered plane wave incident field was used. Unless otherwise noted, the surface realizations were 80 λ in length with 10 partitions per wavelength. We begin with small kh, followed by steadily increasing values.

Figure 4 shows the results for $kh = 0.1$. The fluctuating curve was obtained with the integral equation method, while the smooth curve is the perturbation theory prediction. Note that the bistatic scattering cross section values are given on a logarithmic (dB) scale. The large peak at a scattering angle of 45° is the coherent component in the specular direction; the perturbation results are for incoherent scattering only. Figure 4(a) shows that the lowest-order standard perturbation result [σ_s^{11}given by Eq. (11)] is accurate for this example, except very close to grazing (near ±90°). For plane wave scattering from an arbitrarily long surface, which is assumed in perturbation theory, the cross section expressed in linear units should approach zero when the scattering angle approaches ±90°. The fact that it does not is one indication that a more complete theory is necessary, as mentioned previously. The integral equation result drops down near grazing, but does not vanish at ±90° because the surface length is just 80 λ. When the surface length is increased, the cross section level at grazing drops further.

Figure 4(b) gives the corresponding result for lowest-order renormalized perturbation theory [Eq. (20)]. The agreement with exact results is again very good. Note that with renormalized perturbation theory, the prediction drops rapidly very close to ±90°. The integral equation result does not have sufficient angular resolution in this region to track the σ^{11} curve. The σ^{22} result from (23) is given in Fig. 4(c). For the parameters of this example, the σ^{22} curve in nearly 20 dB below

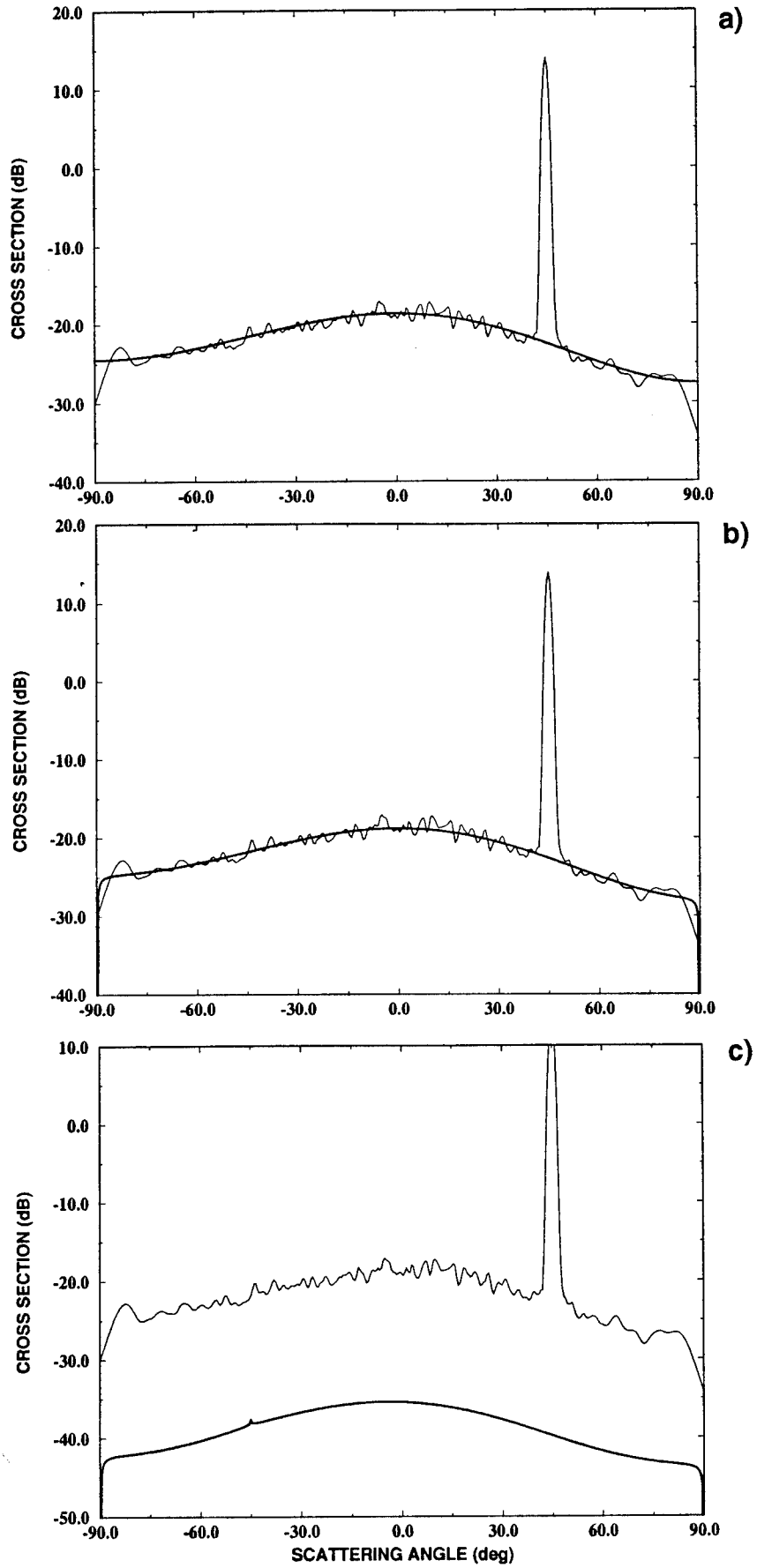

Figure 4. Perturbation theory compared with integral equation results (fluctuating curve) for a perfect conductor with kh = 0.1, kl = 1.0, and θ_i = 45°: (a) σ_s^{11}, (b) σ^{11}, (c) σ^{22}. Renormalized perturbation theory has been used, except when the subscript s indicates standard perturbation theory.

the σ^{11} curve and can be safely neglected. (The σ^{13} curve is even further below.) Note, however, the small backscattering enhancement peak in the backscattering direction (–45°). The enhancement here is due to the coherent addition of reciprocal double-scattering paths, where the intermediate state is dominated by a roughness induced surface wave.

For Fig. 5, *kh* has been increased to 0.2, all other parameters remaining the same. Standard perturbation theory, Fig. 5(a), is now slightly high but still quite good. Recall that with standard perturbation theory only the lowest order, σ_s^{11}, gives finite results, so this series cannot be extended. The renormalized σ^{11} remains in good agreement with exact results, as shown in Fig. 5(b), though adding the σ^{22} term [Fig. 5(c)] does give slight improvement in the forward scattering region near the specular direction.

In Fig. 6, *kh* has been increased to 0.3. The surface length was also increased to 160 λ, which gives improved angular resolution. The result for σ_s^{11} [Fig. 6(a)] has more noticeable error than in the previous example, and at this level of roughness the accuracy of the renormalized σ^{11} [Fig. 6(b)] has also degraded. The result for σ^{11} is about as much low as σ_s^{11} is high when represented on a logarithmic scale, and this pattern continues at higher levels of roughness. It is very reassuring that when σ^{22} is included [Fig. 6(c)] the agreement is excellent. This shows that the renormalization has properly converted the infinite σ_s^{22} term into a quantity that accurately corrects the error in σ^{11} for this example. The addition of σ^{13} does not cause a noticeable change to the result shown in Fig. 6(c).

Figures 7 and 8 give the results for $kh = 0.4$ and 0.5, respectively. The error for σ^{11} is about the same as that shown in Figs. 7(a) and 8(a) for σ_s^{11}, but of opposite sign, and is not shown. Examination of the (b) and (c) panels of these figures shows that the goal of implementing a renormalized perturbation theory valid up to a *kh* of 0.5 has been essentially reached. For all of the examples discussed so far, the self-energy was computed according to (22). Therefore, as discussed in Section 3.1.4, the Ward identity is not satisfied when σ^{22} and/or σ^{13} are included.

Though the agreement shown in Figs. 7(c) and 8(c) between renormalized perturbation theory and exact results is very good, there is a little room for improvement, somewhat more noticeable in Fig. 8(c). The perturbation theory calculations were redone using the fourth-order self-energy [Eq.(34)] to see if satisfaction of the Ward identity would bring the results into even better agreement. The results are shown in Fig. 9. When $kh = 0.4$, the agreement is quite good in both Figs. 7(c) and 9(a), and little can be concluded from this comparison. When $kh = 0.5$, the agreement with the Ward identity satisfied [Fig. 9(b)] is improved in the forward region near the specular peak in comparison with the agreement when it is not satisfied [Fig. 8(c)], but is not as good in the back region. For these cases, there is no real advantage in going through the extra work of upgrading the self-energy in order that the Ward identity is satisfied to fourth order. This can be viewed as a good result, lessening the complexity of extending these methods to other problems, such as scattering from good conductors or from 2-D surfaces. It should be recognized, however, that to achieve the success with renormalized perturbation theory shown here, the self-energy was required at the full level defined by (22). Further approximation to (22) in order to avoid solution of the nonlinear integral equation did not yield satisfactory results.

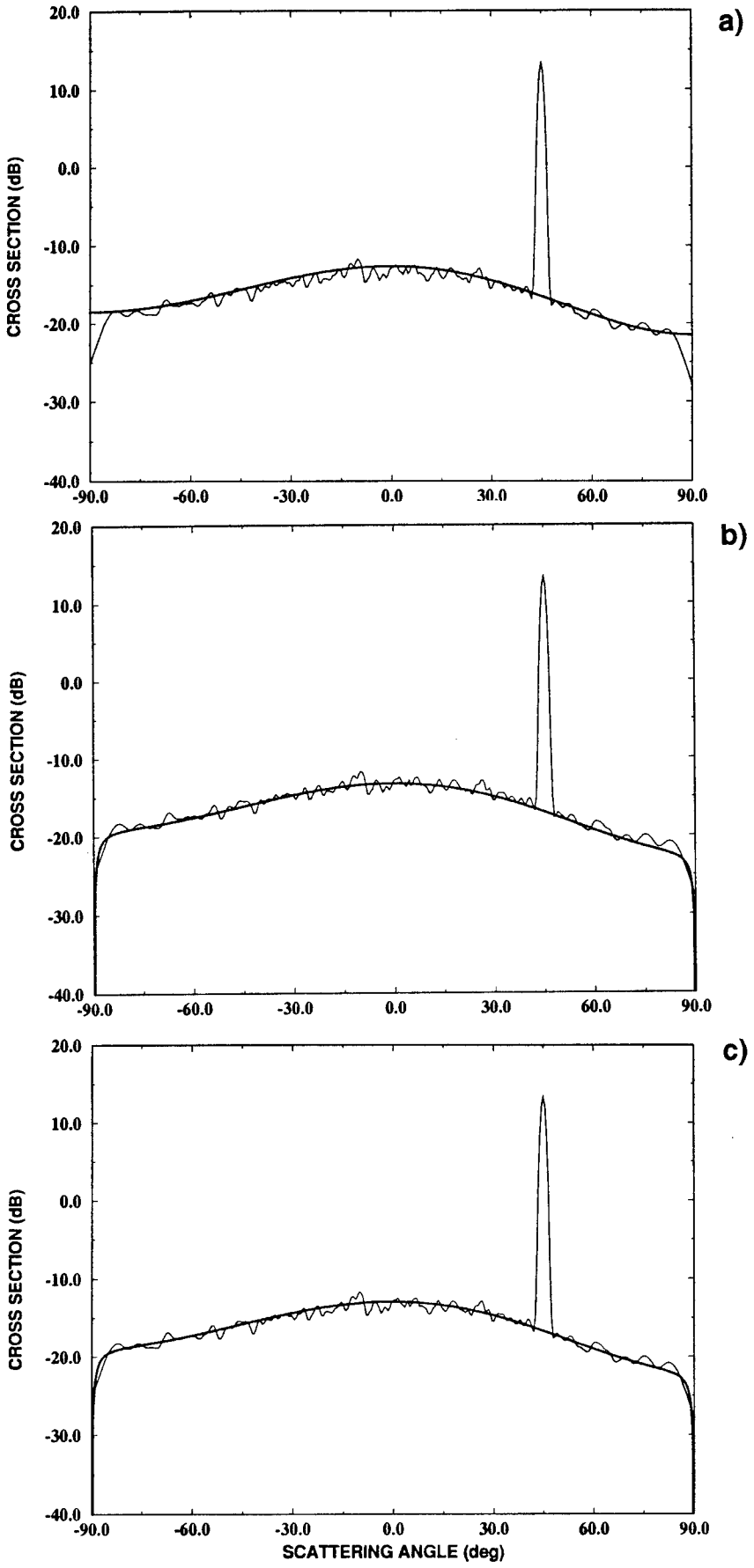

Figure 5. Perturbation theory for kh = 0.2, with other parameters unchanged: (a) σ_s^{11}, (b) σ^{11}, (c) $\sigma^{11} + \sigma^{22}$.

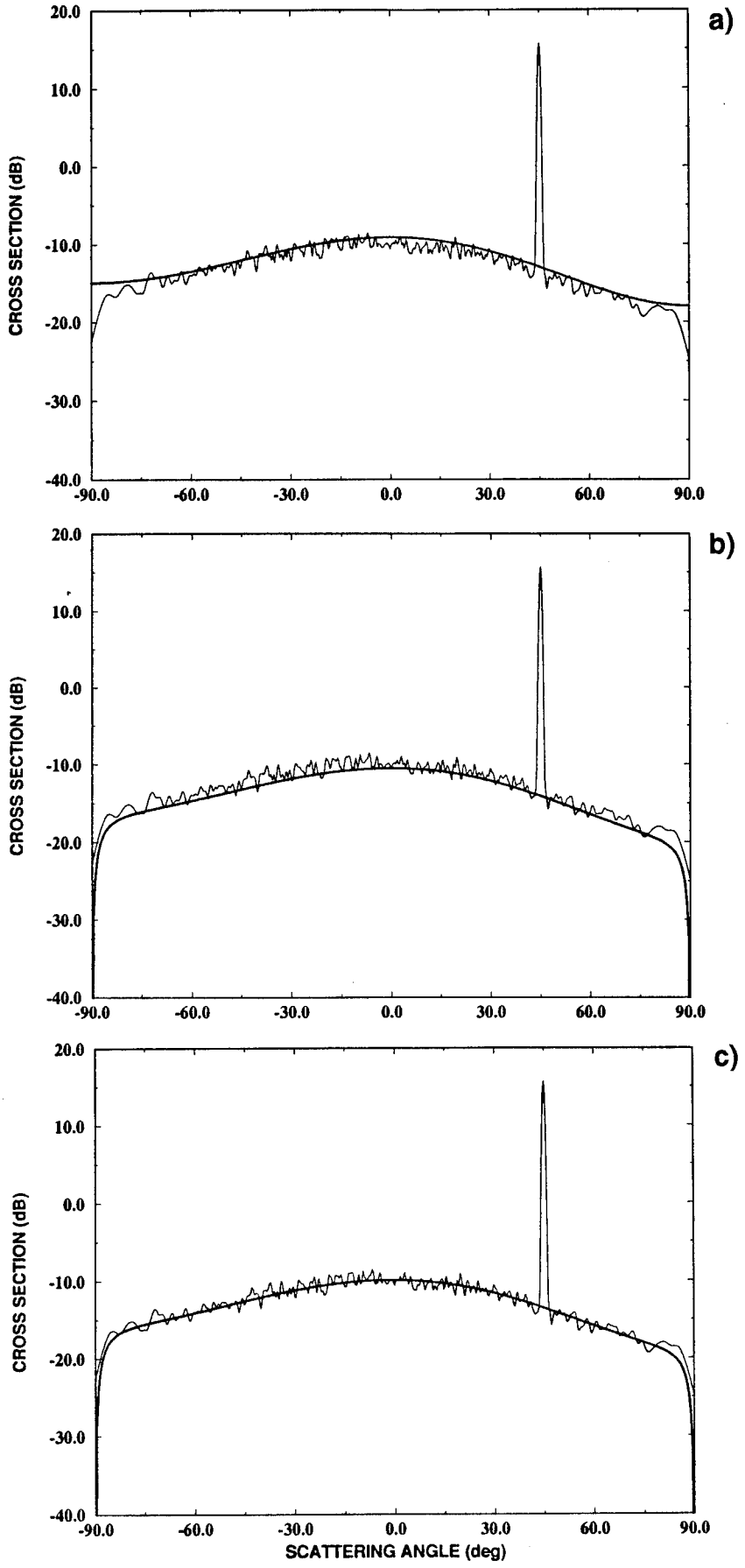

Figure 6. Perturbation theory for kh = 0.3, with other parameters unchanged: (a) σ_s^{11}, (b) σ^{11}, (c) $\sigma^{11} + \sigma^{22}$.

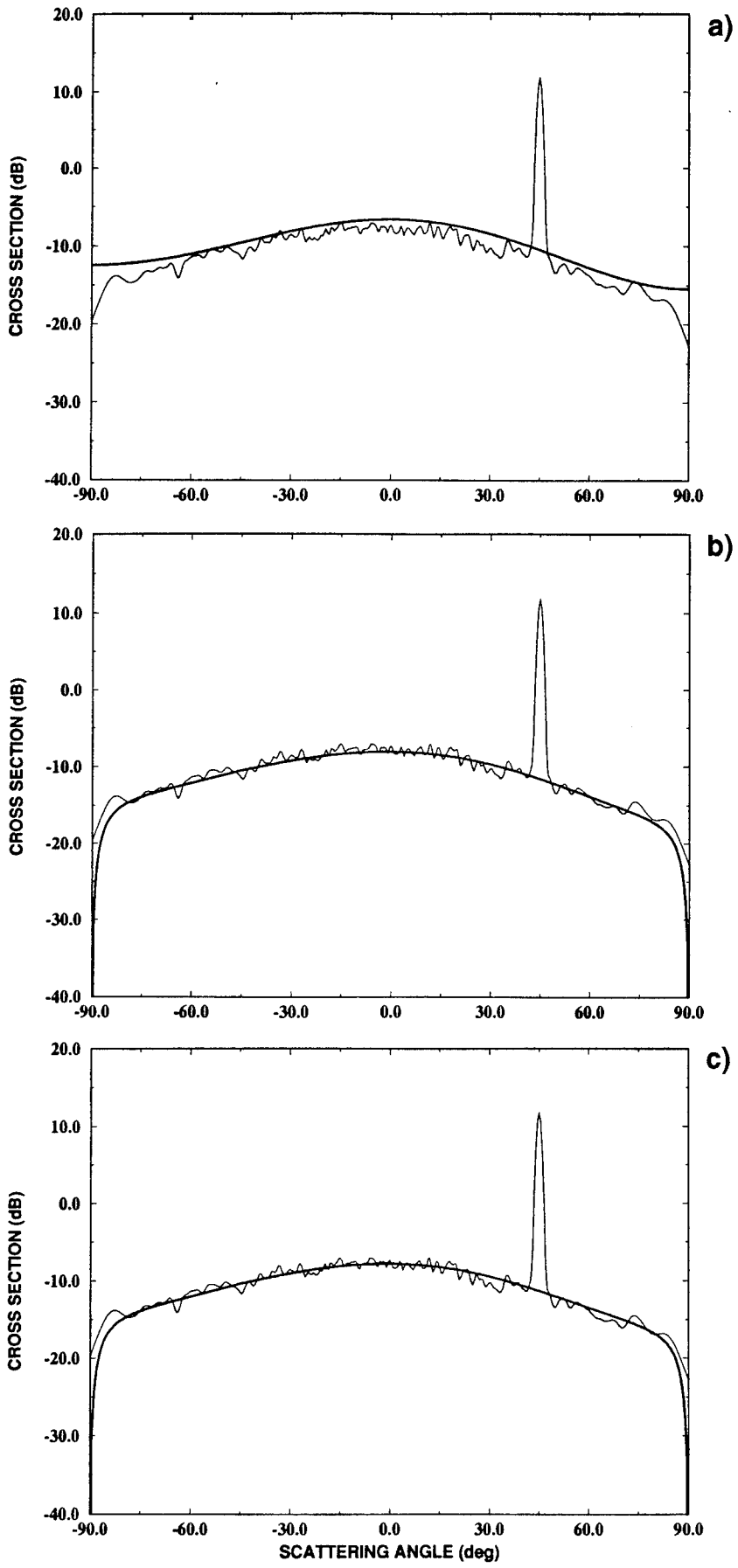

Figure 7. Perturbation theory for kh = 0.4, with other parameters unchanged: (a) σ_s^{11}, (b) $\sigma^{11}+\sigma^{22}$, (c) $\sigma^{11}+\sigma^{22}+\sigma^{13}$.

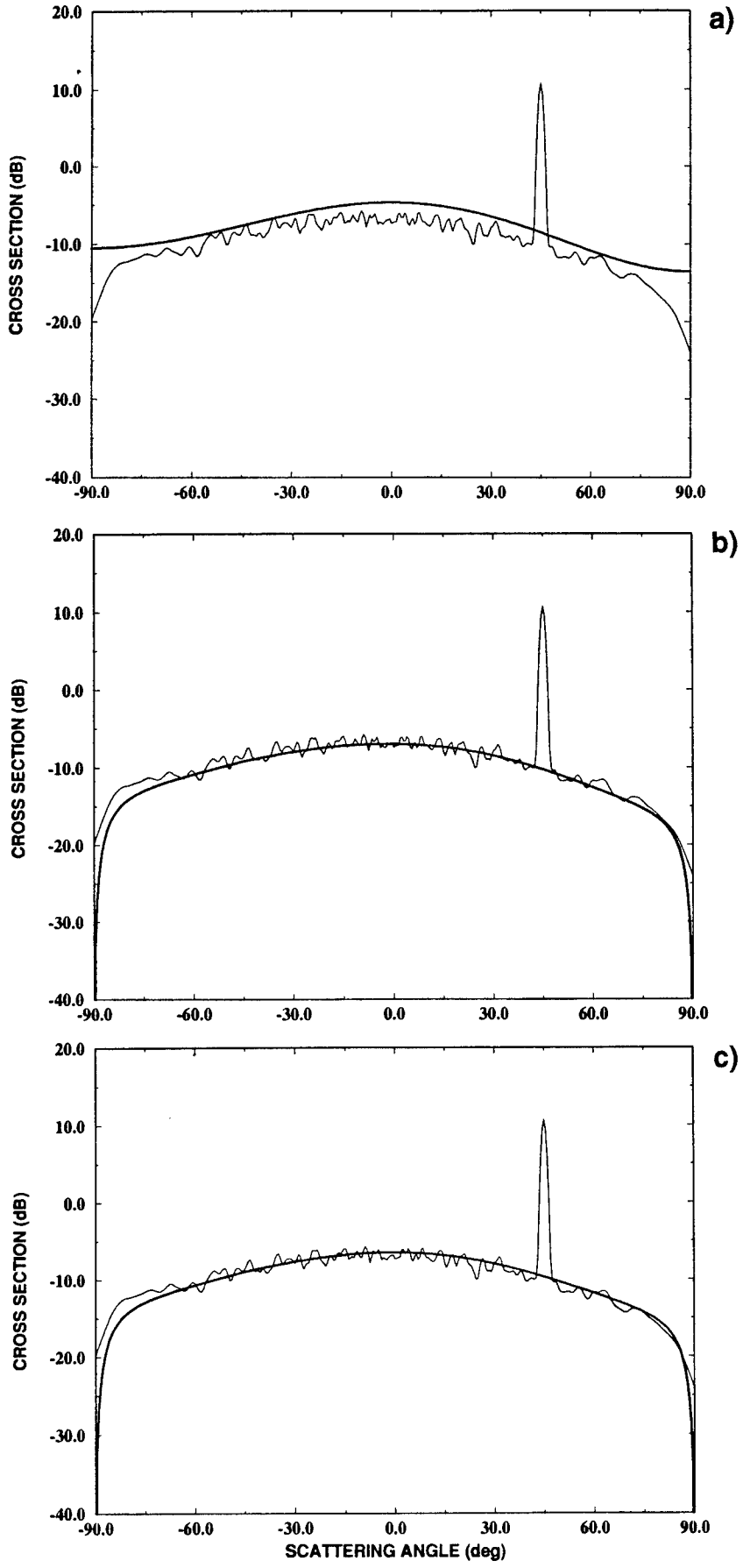

Figure 8. Perturbation theory for kh = 0.5, with other parameters unchanged: (a) σ_s^{11}, (b) $\sigma^{11}+\sigma^{22}$, (c) $\sigma^{11}+\sigma^{22}+\sigma^{13}$.

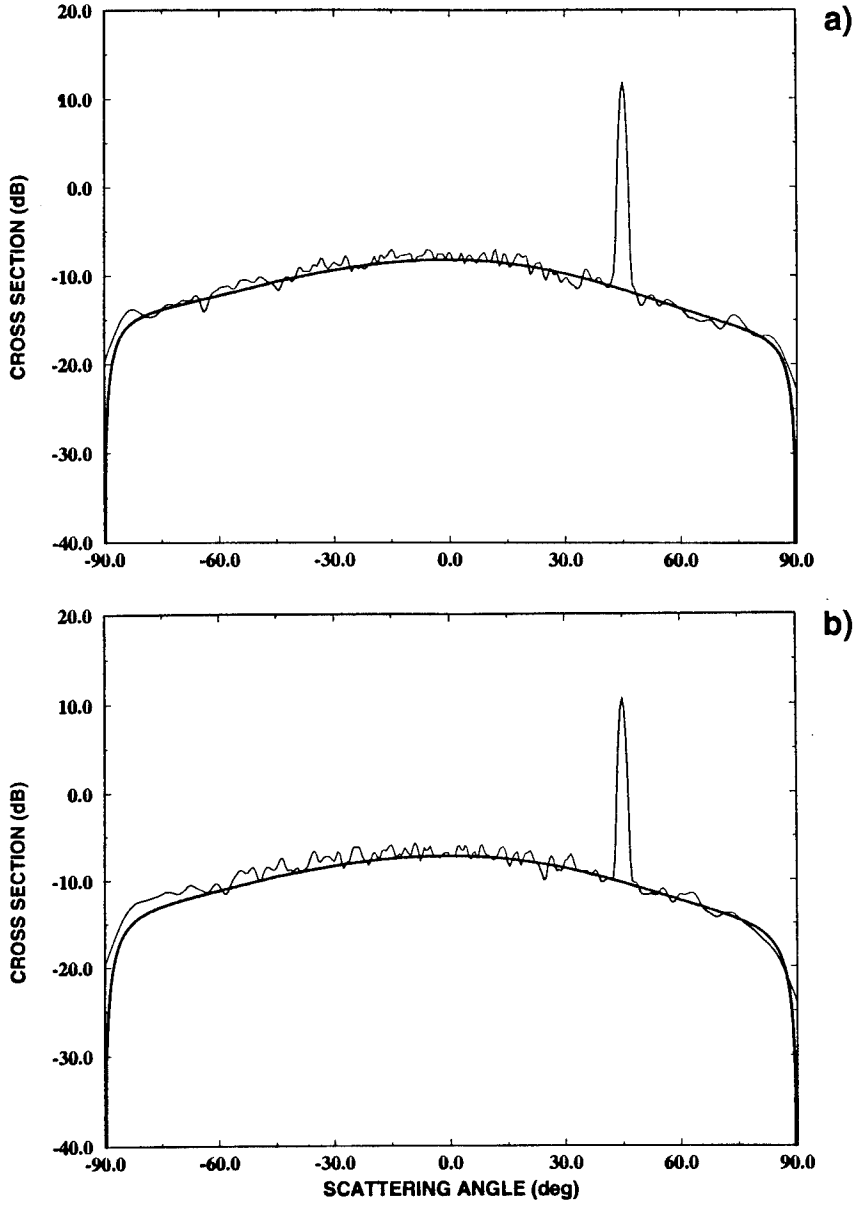

Figure 9. Perturbation theory result for $\sigma^{11}+\sigma^{22}+\sigma^{13}$ when the Ward identity is satisfied to fourth order using the self-energy given by Eq. (34): (a) kh = 0.4, (b) kh = 0.5.

4. Summary

Research has been conducted in two related areas for p-polarized scattering from conducting surfaces: (1) the generation of surface waves, and (2) the development of renormalized perturbation theory for scattering from perfectly conducting surfaces.

To understand the excitation of surface waves better, a numerical method was developed for visualizing the electromagnetic field near rough surfaces, as illustrated in Figs. 1–3. The method is based on integral equation solutions, and no fundamental approximations are required. Field visualization should be very useful for gaining physical insight into complex scattering phenomena where theoretical approaches may be insufficient. Thus this method has the potential for improving our understanding of scattering phenomena in some applied problems.

The existence of electromagnetic surface waves is related to an increase in the complexity of theoretical treatments of p-polarized scattering. We have specialized to scattering from perfectly conducting surfaces with relatively small roughness and developed an implementation of renormalized perturbation theory that extends the work of previous investigators. The accuracy of the method was compared with exact numerical results, showing that our implementation yields accurate results beyond the range of previous efforts. The work in this project is one step in the more general task of developing robust scattering models for 2-D surfaces with arbitrary conductivity.

References

1. J. M. Soto-Crespo, M. Nieto-Vesperinas, and A. T. Friberg, "Scattering from slightly rough random surfaces: A detailed study on the validity of the small perturbation method," J. Opt. Soc. Am. A **7**, 1185–1201 (1990).

2. G. Brown, V. Celli, M. Haller, A. A. Maradudin, and A. Marvin, "Resonant light scattering from a randomly rough surface," Phys. Rev. B **31**, 4993–5005 (1985).

3. V. Celli, A. A. Maradudin, A. M. Marvin, and A. R. McGurn, "Some aspects of light scattering from a randomly rough metal surface," J. Opt. Soc. Am. A **2**, 2225–2239 (1985).

4. A. R. McGurn, A. A. Maradudin, and V. Celli, "Localization effects in the scattering of light from a randomly rough grating," Phys. Rev. B **31**, 4866–4871 (1985).

5. A. A. Maradudin, "The scattering of p-polarized light from a slightly rough perfectly conducting one-dimensional surface," in *Theories of Matter,* edited by A. Solomon, World Scientific, Singapore, pp. 141–171 (1994).

6. E. I. Thorsos and D. R. Jackson, "The validity of the perturbation approximation for rough surface scattering using a Gaussian roughness spectrum," J. Acoust. Soc. Am. **86**, 261–277 (1989).

7. A. A. Maradudin, T. Michel, A. R. McGurn, and E. R. Mendez, "Enhanced backscattering of light from a random grating," Annals of Physics **203**, 255–307 (1990).

8. E. I. Thorsos, "The validity of the Kirchhoff approximation for rough surface scattering using a Gaussian roughness spectrum," J. Acoust. Soc. Am. **83**, 78–92 (1988).

9. R. Garcia-Molina, A. A. Maradudin, and T. A. Leskova, "The impedance boundary condition for a curved surface," Physics Reports **194**, 351–359 (1990).